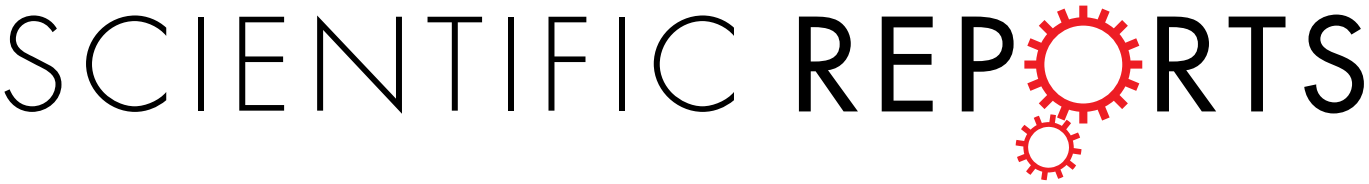

OPEN

Received: 24 January 2017
Accepted: 07 March 2017
Published: 04 April 2017

Meissner effect measurement of single indium particle using a customized on-chip nano-scale superconducting quantum interference device system

Long Wu[1,2], Lei Chen[1,2], Hao Wang[1,2], Xiaoyu Liu[1,2] & Zhen Wang[1,2,3]

As many emergent phenomena of superconductivity appear on a smaller scale and at lower dimension, commercial magnetic property measurement systems (MPMSs) no longer provide the sensitivity necessary to study the Meissner effect of small superconductors. The nano-scale superconducting quantum interference device (nano-SQUID) is considered one of the most sensitive magnetic sensors for the magnetic characterization of mesoscopic or microscopic samples. Here, we develop a customized on-chip nano-SQUID measurement system based on a pulsed current biasing method. The noise performance of our system is approximately 4.6×10^{-17} emu/Hz$^{1/2}$, representing an improvement of 9 orders of magnitude compared with that of a commercial MPMS (~10^{-8} emu/Hz$^{1/2}$). Furthermore, we demonstrate the measurement of the Meissner effect of a single indium (In) particle (of 47 μm in diameter) using our on-chip nano-SQUID system. The system enables the observation of the prompt superconducting transition of the Meissner effect of a single In particle, thereby providing more accurate characterization of the critical field H_c and temperature T_c. In addition, the retrapping field H_{re} as a function of temperature T of single In particle shows disparate behavior from that of a large ensemble.

The zero resistivity and Meissner effect are two of the most fundamental properties of superconductivity[1], and both are crucial for identifying and studying superconducting materials. The zero resistivity can be simply characterized using an electrical transport measurement. The measurement of Meissner effect, which is sometime considered to be a more essential characterization and implies the zero resistivity, is indirect and therefore more complex. A commercial magnetic property measurement system (MPMS) based on a superconducting quantum interference device (SQUID) has been developed and widely used by many researchers[2]. Since such a system couples the sample to a distant SQUID through a pickup coil, a large sample size is required for appropriate characterization of the magnetic properties. However, as many emergent superconductivity phenomena appears on a smaller scale or at lower dimension[3–7], such as the paramagnetic Meissner effect in small superconductors[3] and the Little–Parks–de Gennes effect in ultra-small Al loops[6]. Therefore, a more sensitive method to measure the Meissner effect is highly desirable.

The sensitivity to magnetic moments of a SQUID can be significantly increased by shrinking down its washer size into nano-scale[8–11]. Because the nano-SQUID can be directly coupled to a small sample in the magnetic field[12–15], it has made a great contribution to the field of nano-magnetism[16–19]. Recently, it was demonstrated that a nano-SQUID can be integrated on the tip of a scanning SQUID microscope to perform high-resolution imaging over a sample surface[20–24]. At the same time, a set of three-axis nano-SQUIDs was integrated on the same chip for directly performing the on-chip measurement of the vector magnetic moment[25]. In this paper, we demonstrate

[1]CAS Center for Excellence in Superconducting Electronics(CENSE), State Key Laboratory of Functional Materials for Informatics, Shanghai Institute of Microsystem and Information Technology (SIMIT), Chinese Academy of Sciences (CAS), Shanghai 200050, China. [2]University of Chinese Academy of Sciences, Beijing 100049, China. [3]School of Physical Science and Technology, Shanghai Tech University, Shanghai 200031, China. Correspondence and requests for materials should be addressed to L.C. (email: leichen@mail.sim.ac.cn) or Z.W. (email: zwang@mail.sim.ac.cn)

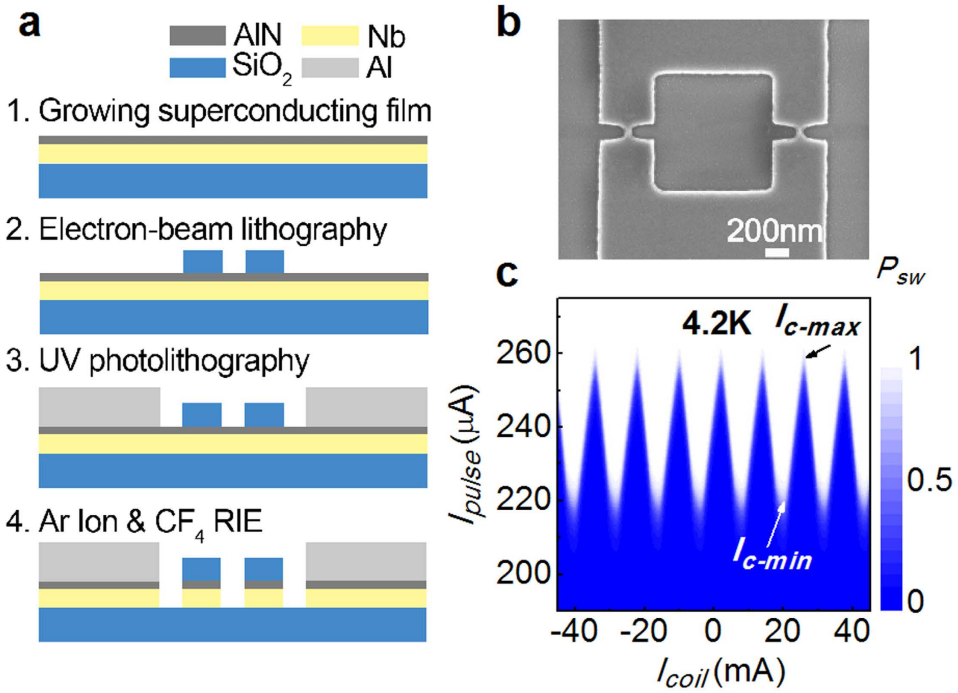

Figure 1. (**a**) Main steps of the nano-SQUID fabrication process. (**b**) SEM image of a typical SQUID; the loop area is 1 μm^2, and the size of the junctions is 60 nm × 75 nm. (**c**) Flux modulation curve of the nano-SQUID.

a simple method to measure the Meissner effect of a single indium (In) particle using a customized on-chip nano-SQUID system. The sensitivity in magnetic moments of our system reaches approximately 4.6×10^{-17} emu/$Hz^{1/2}$, compared with that of a commercial MPMS (10^{-8} emu/$Hz^{1/2}$)[2], which represents an improvement of 9 orders of magnitude. Furthermore, our system observed a prompt superconducting transition of the Meissner effect, and thereby delivers a more accurate critical field H_c and critical temperature T_c compared with the measurement of a large ensemble by the MPMS. In addition, the behavior of the re-trapping field H_{re} as a function of temperature T for single In particle differs from that of a large ensemble. The disparate behavior is probably attributed to the large surface-to-volume ratio of the single particle leading to enhanced behavior of the surface states. We believe that our system will potentially lead to many promising discoveries that occur on a smaller scale or at a lower dimension in the emergent superconductivity field.

Methods

Nano-SQUID fabrication. The main fabrication process for our nano-SQUIDs is schematically illustrated in Fig. 1(a). The process starts with the growth of a 15 nm-thick niobium (Nb) film using direct-current magnetron sputtering on a Si substrate coated with a 400 nm-thick layer of silicon dioxide (SiO_2). Then, a 2 nm-thick aluminum nitride (AlN) layer is grown *in-situ* on top of the Nb film to protect it from oxidation. Next, the nano-SQUID is patterned using a negative resist (XR1541-002) for electron beam lithography (EBL). After that, the nano-SQUID is electrically led out to contact pads using an ultraviolet(UV) photolithography step. Finally, a reactive ion etching (RIE) process is used to remove the unwanted part of the Nb/AlN film to form the nano-SQUID, as it is shown in Fig. 1(b). Compared to our previous process[26], the using of the negative EBL resist avoids a troublesome lift-off step and increases the yields of SQUIDs. In Fig. 1(c), the critical current (I_c) of a nano-SQUID is plotted as a function of the applied magnetic flux. The flux modulation depth (*FMD*) of the nano-SQUID is 14% at 4.2 K. Here, the *FMD* is defined as $FMD = (I_{c\text{-}max} - I_{c\text{-}min})/I_{c\text{-}max}$, where the $I_{c\text{-}max}$ and $I_{c\text{-}min}$ represent I_c at the constructive and destructive quantum interference, respectively.

On-chip SQUID measurement system. Our on-chip nano-SQUID measurement system is schematically illustrated in Fig. 2. The nano-SQUID chip was mounted on a chip carrier fixed onto the cold finger of a variable temperature insert (VTI). Above the chip carrier, a small hand-wound superconducting feedback coil was placed to flux bias the SQUID. The entire VTI was inserted into the middle of a superconducting magnet, which can provide a large parallel magnetic field $H_{//}$. The single particle was placed on the chip near the SQUID loop to provide optimal coupling.

Because a the planar nano-SQUID usually shows a hysteretic current–voltage (*I-V*) curve, we used a pulsed current bias method to obtain the readout such that the SQUID was reset to zero bias at the end of each current pulse. We also assembled a field-programmable-gate-array (FPGA) based SQUID readout system to perform a fast measurement as illustrated in Fig. 2. The pulsed current bias method works as follows. A constant number N_{pulse} of current pulses of amplitude I_{pulse} was sent to a nano-SQUID using a waveform generator (NI PXIe-6555) in series with a large resistance $R = 4\,k\Omega$. The width of generated pulse is 1.6 μs with a repetition frequency of

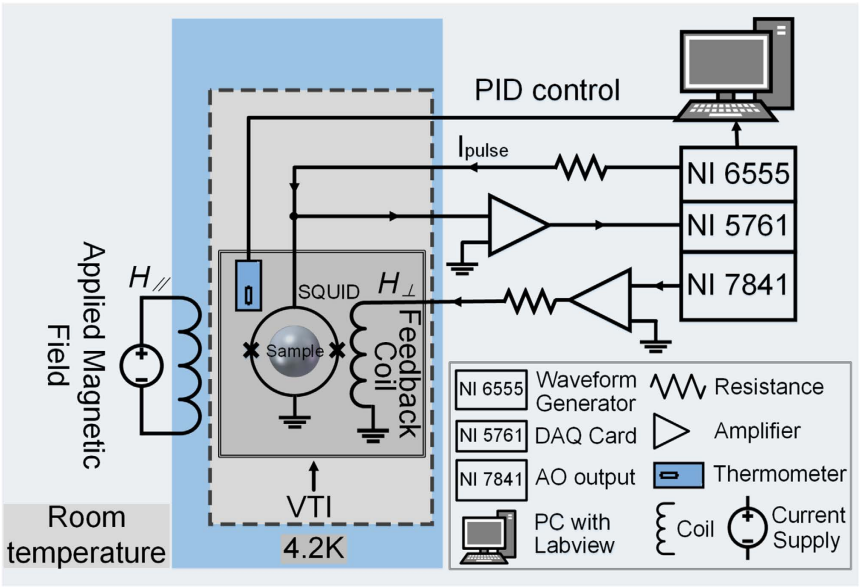

Figure 2. The schematic diagram of the on-chip nano-SQUID measurement system.

250 kHz. Then, the corresponding voltage pulses V_{sw_i} across the SQUID was collected using a high speed analog data acquisition card (DAQ NI 5761) in connection with a room-temperature preamplifier. The voltage pulse number N_{sw} was counted by the V_{sw_i} greater than a threshold voltage V_{th}. The on-board FPGA circuit was programmed to detect the corresponding voltage pulse and calculate the switching probability $P_{sw} = N_{sw}/N_{pulse}$ and average pulse height $V_{sw} = \Sigma V_{sw\_i}/N_{pulse}$. Then, based on the P_{sw} or V_{sw}, the FPGA locked the SQUID by tuning the analog output current (NI PXI-7841R) to the feedback coil to compensate for the flux variation. In this manner, the entire SQUID feedback process was performed by the FPGA without talking to the computer. The current pulse could be as short as 500 ns and was limited by the bandwidth of the wires connected to the SQUID.

Results and Discussion

Characterization of system noise. Because a low-noise measurement system is essential for characterizing the magnetic properties of small samples, we evaluated the noise performance of our on-chip nano-SQUID measurement system in terms of both P_{sw} and V_{sw}, as shown in Fig. 3. The inset of Fig. 3(b) demonstrates that both P_{sw} and V_{sw} were periodically modulated by I_{coil} at a bias of $I_{pulse} = 239\,\mu A$. In order to characterize the flux noise, the flux bias of the SQUID was fixed at $I_{coil} = 3.75$ mA, as indicated by the the blue point in the inset of Fig. 3(b). By measuring P_{sw} and V_{sw} as a function of time t and converting the data into the frequency domain by using of a fast Fourier transform, the noise density spectra S_{Psw} and S_{Vsw} were obtained. As observed in the Fig. 3(a), the flux noise density spectrum $S(\Phi)_{Psw(Vsw)} = \Phi_0/I_{coil}^{period} \times \delta\Phi/\delta P_{sw}(\delta V_{sw}) \times S_{Psw}(S_{Vsw})$, where $I_{coil}^{period} = 13.9$ mA corresponds to the current in the feedback coil generating a single flux quanta Φ_0 to the SQUID, and $\delta\Phi/\delta P_{sw}(\delta V_{sw})$ is the inverse of the derivative at the blue point of the P_{sw} (V_{sw}) modulation curve in the inset of Fig. 3(b). For $N_{pulse} = 1000$, the white flux noise was determined to be 74.4 and $53.6\,\mu\Phi_0/Hz^{1/2}$ at 4.2 K by measuring P_{sw} and V_{sw} respectively. Although the white flux noise determined by measuring P_{sw} was slightly greater than that determined by measuring V_{sw}, the low-frequency part obtained by measuring P_{sw} was much better. Therefore, a lower noise floor was achieved by measuring P_{sw} for the slow measurement such as the magnetization curve of sweeping the magnetic field. The flux noise density on the log scale also improved linearly upon increasing $N_{pulse}^{1/2}$ as observed in Fig. 3(b). For $N = 10^4$, the white flux noise determined by measuring P_{sw} reached $28\,\mu\Phi_0/Hz^{1/2}$, with a corresponding sensitivity in magnetic moments of approximately 4.6×10^{-17} emu/Hz$^{1/2}$ [8,27,28]. Compared with the value for a commercial MPMS system (Quantum Design MPMS-3) of 1.0×10^{-8} emu/Hz$^{1/2}$, our on-chip SQUID measurement system showed an improvement of 9 orders of magnitude.

In principle, the intrinsic flux noise of nano-SQUIDs may approach the quantum limit because of its ultra-low inductance[9]. Several state-of-the-art nano-SQUIDs have already achieved the intrinsic flux noise below $50\,n\Phi_0/Hz^{1/2}$, such as the Pb nano-SQUID-on-tip[29], the YBCO nano-SQUID made by the focused ion beam[30,31], the Al 3D nano-SQUID made by the shadow evaporation[32], etc. Recently, we also made Nb 3D nano-SQUID with the intrinsic flux noise of $340\,n\Phi_0/Hz^{1/2}$ [13]. The planar Nb nano-SQUID in Fig. 1(b) do have a large intrinsic flux noise because of its large inductance, but can be operated in a high parallel magnetic field[12]. However, the system noise of $28\,\mu\Phi_0/Hz^{1/2}$ has been limited by the room-temperature amplifier and not reached its intrinsic noise level yet. Therefore, the improvement of another two orders of magnitude in the sensitivity of magnetic moments can be optimistically expected.

On-chip Meissner effect measurement of a single In particle. For demonstration, we measured the Meissner effect of a single indium (In) particle. The single In particle was placed on the SQUID chip, as shown in the inset of Fig. 4(a), and cooled to low temperature by the VTI. The SQUID was locked at its working point by the FPGA-controlled readout system as described in the section of Methods. Then, by slowly sweeping

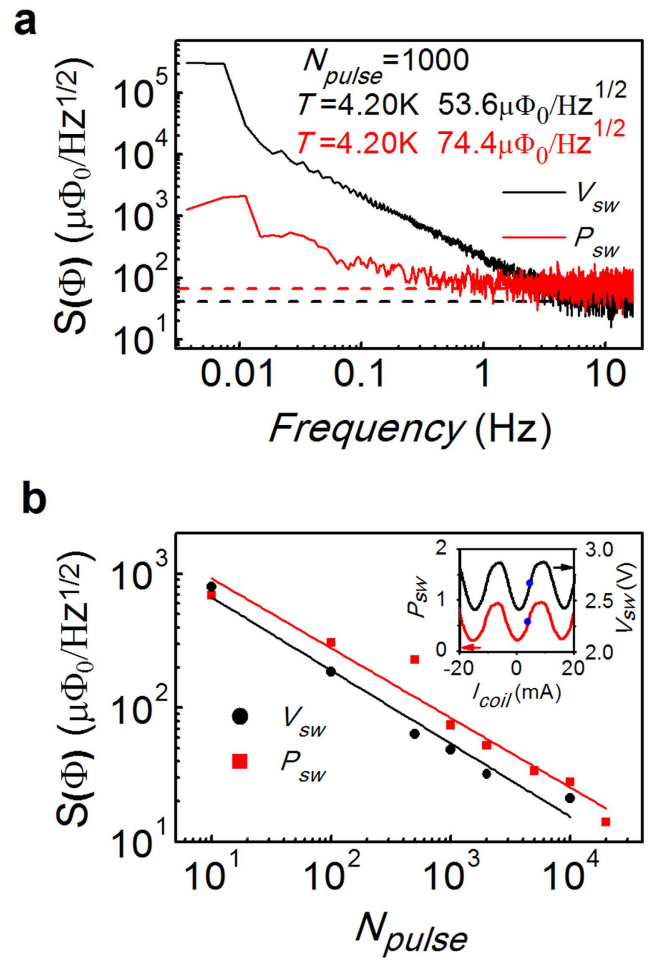

Figure 3. (**a**) Flux noise density spectra obtained by measuring P_{sw} (red curve) and V_{sw} (black curve) respectively for $N_{pulse} = 1000$. (**b**) White flux noise density for various number of pulses N_{pulse} by measuring P_{sw} (red squres) and V_{sw} (black dots). The solid lines are linear fits to a function of $N_{pulse}^{1/2}$. The inset shows both P_{sw} (red) and V_{sw} (black) of the SQUID as a function of the feedback coil current and the working points (blue points) where the flux noise density spectra were measured.

the magnetic field $H_{//}$, the magnetic flux variation generated by the Meissner effect of the single In particle was directly picked up by the on-chip SQUID. As illustrated in Fig. 4(a), by ramping up the $H_{//}$, the sample switched from a diamagnetic branch to zero magnetization at the field H_c, which indicated that the In particle switched from the superconducting to normal state. As the field ramped down, the In particle was re-trapped back to the diamagnetic branch at a lower field H_{re}. The magnetization M as a function of temperature T, at various $H_{//}$, is also plotted in Fig. 4(b). M generated by the superconducting Meissner effect switches back to the normal state at $T = T_c$. In Fig. 4(c), the H_c and H_{re} are plotted as a function of T.

For comparison, Fig. 4(d,e) present Meissner effect measurements of the In particles in a large ensemble (approximately 61,000 particles with diameters of 30–50 μm) by using of the commercial MPMS. In Fig. 4(d), the M-H measurement of the large ensemble clearly shows a smeared-out transition between the superconducting and normal state. The transition of M at T_c is also broadened. In contrast, the single In particle measured by the on-chip SQUID system showed a much prompt transition, which is expected for a Type I superconductor. The broadened or smeared–out transition observed in the particle ensemble might originate from the variation of the individual particles or a clustering effect that distorts the local magnetic field for each particle. Therefore, the on-chip SQUID measurement delivers a more accurate characterization at H_c and T_c. Moreover, the H_{re} -T curve of a single In particle in Fig. 4(c) has a different slope than the H_c –T curve. For the large ensemble, the slope of the H_{re}-T curve is approximately equal to that of the H_c-T curve. H_{re} is believed to be related to a super-cooling process[33,34], in which the nucleation center near the surface prevents the forming of superconducting phase below H_c by lowering the magnetic field. Furthermore, the super-cooling effect is supposed to decrease as T approaches T_c because the coherence length and the penetration depth diverges at T_c. Therefore, the disparate H_{re}-T behavior of a single In particle from the large ensemble reveals more information about the surface state of small superconductors. Therefore, we believe that our system is a powerful tool to study the emergent phenomena of superconductivity that occur on a smaller scale or at a lower dimension.

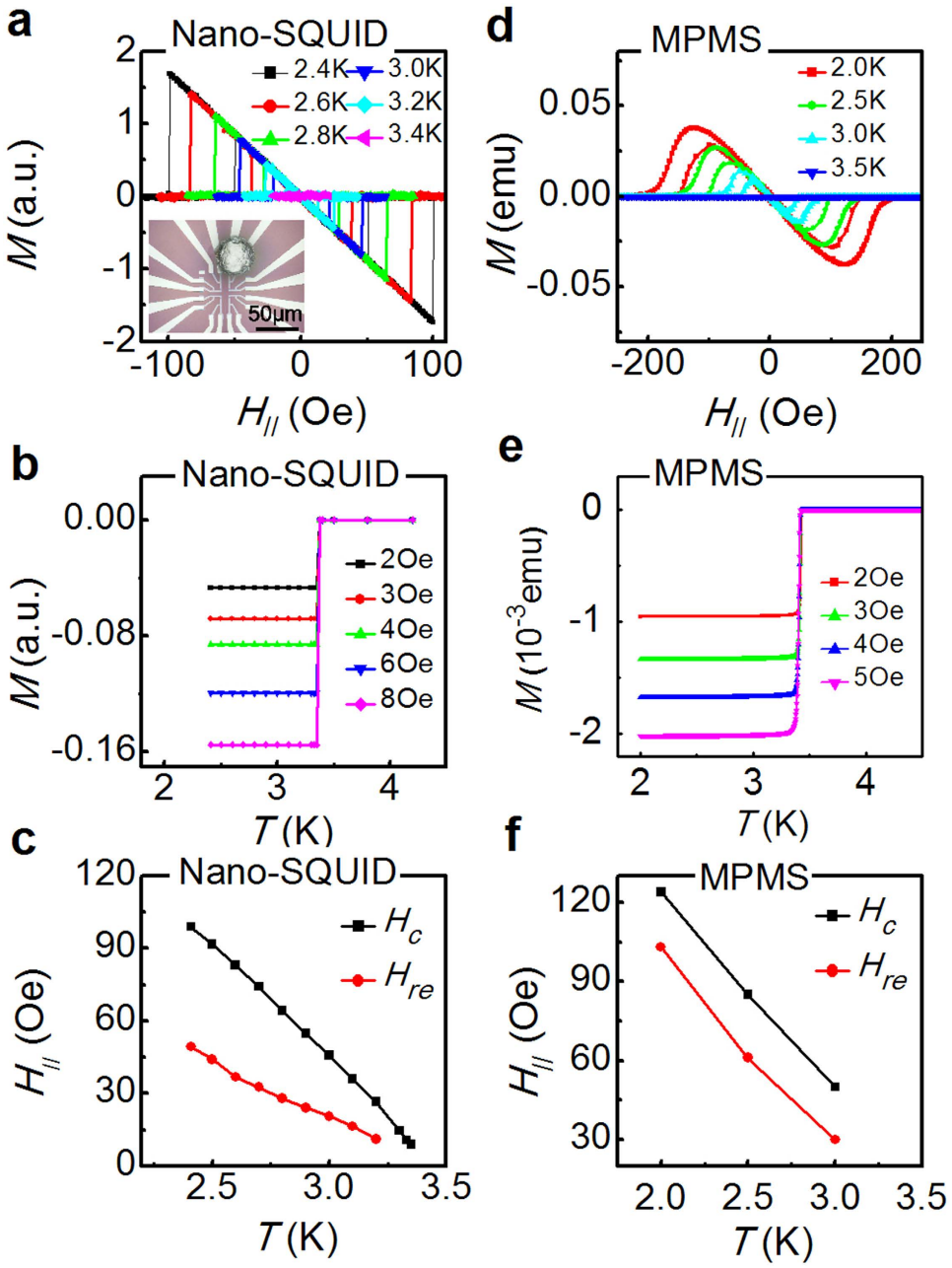

Figure 4. (**a**) M as a function of applied magnetic field $H_{//}$ of a single In particle measured by the on-chip SQUID system at various temperatures. (**b**) M as a function of T of a single In particle measured by the on-chip SQUID system at various $H_{//}$. (**c**) H_c (black squares) and H_{re} (red dots) as a function of the T from Figure 4(a). (**d**) The M-$H_{//}$ curve of a large ensemble of In particles (approximately 61,000 particles) measured by the MPMS at various T. (**e**) M-T curve of a large ensemble of In particles measured by the MPMS system. (**f**) H_c (black squares) and H_{re} (red dots) as a function of T from Figure 4(d).

Conclusion

In order to measure the Meissner effect of small superconductors, we developed a simple process for fabricating planar Nb nano-SQUIDs based on a negative EBL resist and constructed an on-chip nano-SQUID measurement system based on a current pulse biasing method and FPGA-controlled feedback. The noise performance of the system reached $S(\Phi)_{Psw} = 28\,\mu\Phi_0/Hz^{1/2}$ (approximately 4.6×10^{-17} emu/$Hz^{1/2}$), which represents an improvement of 9 orders of magnitude compared with that of a commercial MPMS system (1.0×10^{-8} emu/$Hz^{1/2}$). Furthermore, we demonstrated the measurement of the Meissner effect of a single In particle using our on-chip nano-SQUID measurement system. The system enabled the observation of the prompt Meissner effect transition of a single In particle and delivered a more accurate characterization at H_c and T_c. In addition, the disparate behavior of retrapping field H_{re} as a function of temperature T of a single In particle compared with that of a large ensemble clearly

indicate the presence of surface nucleation center only by the on-chip nano-SQUID measurement. Therefore, we believe that our system is a powerful tool to study the emergent phenomena of superconductivity that occur on a smaller scale or at a lower dimension.

References

1. Tinkham, M. *Introduction to superconductivity.* 2nd edn, (McGraw Hill, 1996).
2. Sawicki, M., Stefanowicz, W. & Ney, A. Sensitive SQUID magnetometry for studying nanomagnetism. *Semicond Sci Tech* **26,** 064006 (2011).
3. Geim, A. K., Dubonos, S. V., Lok, J. G. S., Henini, M. & Maan, J. C. Paramagnetic Meissner effect in small superconductors. *Nature* **396,** 144–146 (1998).
4. Bose, S. *et al.* Observation of shell effects in superconducting nanoparticles of Sn. *Nat Mater* **9,** 550–554 (2010).
5. Jang, J. *et al.* Observation of Half-Height Magnetization Steps in Sr2RuO4. *Science* **331,** 186 (2011).
6. Staley, N. E. & Liu, Y. Manipulating superconducting fluctuations by the Little–Parks–de Gennes effect in ultrasmall Al loops. *Proceedings of the National Academy of Sciences* **109,** 14819–14823 (2012).
7. Jiang, D. *et al.* High-Tc superconductivity in ultrathin Bi2Sr2CaCu2O8 + x down to half-unit-cell thickness by protection with graphene. *Nature communications* **5,** 5708 (2014).
8. Ketchen, M. B. *et al.* Design, fabrication, and performance of integrated miniature SQUID susceptometers. *Magnetics, IEEE Transactions on* **25,** 1212–1215 (1989).
9. Granata, C. & Vettoliere, A. Nano Superconducting Quantum Interference device: A powerful tool for nanoscale investigations. *Physics Reports* **614,** 1–69 (2016).
10. Bouchiat, V. Detection of magnetic moments using a nano-SQUID: limits of resolution and sensitivity in near-field SQUID magnetometry. *Superconductor Science and Technology* **22,** 064002 (2009).
11. Foley, C. P. & Hilgenkamp, H. Why NanoSQUIDs are important: an introduction to the focus issue. *Superconductor Science and Technology* **22,** 064001 (2009).
12. Chen, L., Wernsdorfer, W., Lampropoulos, C., Christou, G. & Chiorescu, I. On-chip SQUID measurements in the presence of high magnetic fields. *Nanotechnology* **21,** 405504 (2010).
13. Chen, L., Wang, H., Liu, X., Wu, L. & Wang, Z. A High-Performance Nb Nano-Superconducting Quantum Interference Device with a Three-Dimensional Structure. *Nano Lett* **16,** 7726–7730 (2016).
14. Antler, N. *et al.* In-plane magnetic field tolerance of a dispersive aluminum nanobridge SQUID magnetometer. *Appl Phys Lett* **102,** 232602 (2013).
15. Wölbing, R. *et al.* Nb nano superconducting quantum interference devices with high spin sensitivity for operation in magnetic fields up to 0.5 T. *Appl Phys Lett* **102,** 192601 (2013).
16. Wernsdorfer, W. From micro- to nano-SQUIDs: applications to nanomagnetism. *Superconductor Science and Technology* **22,** 064013 (2009).
17. Faucher, M., Jubert, P. O., Fruchart, O., Wernsdorfer, W. & Bouchiat, V. Optimizing the flux coupling between a nanoSQUID and a magnetic particle using atomic force microscope nanolithography. *Superconductor Science and Technology* **22,** 064010 (2009).
18. Cleuziou, J. P., Wernsdorfer, W., Bouchiat, V., Ondarcuhu, T. & Monthioux, M. Carbon nanotube superconducting quantum interference device. *Nat Nanotechnol* **1,** 53–59 (2006).
19. Hao, L. *et al.* Detection of single magnetic nanobead with a nano-superconducting quantum interference device. *Appl Phys Lett* **98,** 092504 (2011).
20. Halbertal, D. *et al.* Nanoscale thermal imaging of dissipation in quantum systems. *Nature* **539,** 407–410 (2016).
21. Finkler, A. *et al.* Self-Aligned Nanoscale SQUID on a Tip. *Nano Lett* **10,** 1046–1049 (2010).
22. Finkler, A. *et al.* Scanning superconducting quantum interference device on a tip for magnetic imaging of nanoscale phenomena. *Rev Sci Instrum* **83,** 073702 (2012).
23. Hasselbach, K. *et al.* High resolution magnetic imaging: MicroSQUID Force Microscopy. *Journal of Physics. Conference Series* **97,** 012330 (2008).
24. Shibata, Y. *et al.* Imaging of current density distributions with a Nb weak-link scanning nano-SQUID microscope. *Scientific Reports* **5,** 15097 (2015).
25. Martínez-Pérez, M. J. *et al.* Three-Axis Vector Nano Superconducting Quantum Interference Device. *ACS Nano* (2016).
26. Liu, X., Liu, X. Y., Wang, H., Chen, L. & Wang, Z. The fabrication and characterization of nano-SQUIDs based on Nb thin films. *Physica C: Superconductivity* **515,** 36 (2015).
27. Lam, S. K. H. & Tilbrook, D. L. Development of a niobium nanosuperconducting quantum interference device for the detection of small spin populations. *Appl Phys Lett* **82,** 1078–1080 (2003).
28. Wölbing, R. *et al.* Optimizing the spin sensitivity of grain boundary junction nanoSQUIDs—towards detection of small spin systems with single-spin resolution. *Superconductor Science and Technology* **27,** 125007 (2014).
29. Vasyukov, D. *et al.* A scanning superconducting quantum interference device with single electron spin sensitivity. *Nat Nano* **8,** 639–644 (2013).
30. Schwarz, T. *et al.* Low-Noise Nano Superconducting Quantum Interference Device Operating in Tesla Magnetic Fields. *ACS Nano* **7,** 844–850 (2013).
31. Schwarz, T. *et al.* Low-Noise YBCO Nano-SQUIDs for Performing Magnetization-Reversal Measurements on Magnetic Nanoparticles. *Physical Review Applied* **3,** 044011 (2015).
32. Levenson-Falk, E. M., Vijay, R., Antler, N. & Siddiqi, I. A dispersive nanoSQUID magnetometer for ultra-low noise, high bandwidth flux detection. *Superconductor Science and Technology* **26,** 055015 (2013).
33. Faber, T. E. The Supercooling Effect in Superconductors Close to the Transition Temperature. *Proceedings of the Royal Society of London. Series A. Mathematical and Physical Sciences* **241,** 531 (1957).
34. Feder, J. & McLachlan, D. S. Hysteresis in the superconducting transition of single spheres of indium. *Solid State Commun* **6,** 23–26 (1968).

Acknowledgements

We acknowledge support from the Strategic Priority Research Program of the Chinese Academy of Sciences (Grant No. XDB04000000), as well as funding from the National Science Foundation of China (Grant No. 61306151).

Author Contributions

L.C. and Z.W. planned the research. L.W., L.C. and H.W. performed the experiments and collected the data. X.L. did the electron-beam lithography. L.W. and L.C. analyzed the data. L.C. and Z.W. wrote the paper. All authors approved the final version of the manuscripts.

Additional Information

Competing Interests: The authors declare no competing financial interests.

How to cite this article: Wu, L. *et al.* Meissner effect measurement of single indium particle using a customized on-chip nano-scale superconducting quantum interference device system. *Sci. Rep.* **7**, 45945; doi: 10.1038/srep45945 (2017).

Publisher's note: Springer Nature remains neutral with regard to jurisdictional claims in published maps and institutional affiliations.